Systematic validation of 3D ground-based radars for tracking birds and bats

Grace Chang[1*¶], Jennifer Pettis Schallert[2¶], Stephanie Schneider[3¶], Rachael Young[1&], Sharon Kramer[3&], Lizette Crooks[4&], Jesse Lewis[5&], and Frank Spada[1&]

[1]Integral Consulting Inc., Santa Barbara, California, United States of America

[2]Integral Consulting Inc., Jupiter, Florida, United States of America

[3]Integral Consulting Inc., Arcata, California, United States of America

[4]Sightir, Inc., Santa Barbara, California, United States of America

[5]DeTect, Inc., Panama City, Florida, United States of America

*Corresponding author

Email: gchang@integral-corp.com

[¶]These authors contributed equally to this work

[&]These authors also contributed equally to this work

Abstract

Ground-based radar (GBR) is increasingly used to quantify bird and bat movement in support of ecological studies, environmental monitoring, and collision risk assessment, yet few studies have systematically validated radar-derived tracks against targets with known positions. We evaluated the performance of two commercially available 3D GBRs using controlled drone flights that were designed to simulate biologically relevant movement patterns ranging from straight-line transiting to highly dynamic chasing behavior. Target detection rate, positional deviation, mean absolute positional deviation, and root mean square deviation were computed for radar-derived positions compared to drone positions across horizontal and vertical dimensions. Both radars successfully detected moving targets and produced georeferenced tracks generally consistent with drone positions within tens of meters. Detection performance varied with radar power, flight trajectory relative to radar orientation, and flight track continuity. Flights near the limits of the radar viewshed and behaviors with dynamic maneuvering produced greater tracking variability. Positional discrepancies were primarily driven by georeferencing uncertainty, and track continuity and smoothness. Drone-radar positional discrepancies in the vertical dimension were generally within estimated drone position uncertainties, supporting the use of 3D GBRs to characterize flight height distributions relevant to collision risk modeling. These findings demonstrate that GBR can provide accurate, quantitative bird and bat movement data at spatial and temporal scales difficult to achieve with visual or optical methods alone, while underscoring the importance of careful siting, georeferencing, and conservative interpretation of tracks near radar viewshed limits or during highly dynamic flight behavior. As infrastructure development continues to expand globally, validated GBR systems can strengthen ecological monitoring and support more defensible decisions that balance infrastructure needs with wildlife conservation.

Introduction

Anthropogenic infrastructure has transformed the airspace used by birds and bats, increasing the need to understand wildlife movement through skyscapes that are now occupied by buildings, bridges, towers, transmission lines, wind turbines, and other elevated structures [1-6]. Although these structures differ in size, shape, and operating characteristics, they pose a common problem: potential collision risk to flying animals. Reliable information on bird and bat behavior, including their 3D flight patterns, flight height and speed, and temporal patterns of activity is essential for assessing collision risk; informing infrastructure design, siting, and operations; supporting environmental permitting; and evaluating effectiveness of mitigation measures [7-10]. Capturing these data at the temporal and spatial scales needed to characterize wildlife movement remains a major challenge for accurate collision risk assessment.

Traditional approaches for characterizing bird and bat movement around infrastructure have relied primarily on ground-, vessel-, or aircraft-based human visual observations and surveys. Human observers remain the foundation of many environmental monitoring programs because they can identify species and document behaviors that are difficult to infer from autonomous, remote sensors. However, human-based visual surveys are inherently constrained by daylight, health and safety concerns (weather, observer fatigue), limited spatial coverage, detection bias, and distance and height estimation errors, often resulting in incomplete or inaccurate characterizations of flight activity (Koger et al. [11] and references therein).

More recently, optical imaging technologies are being deployed from observing stations or crewed or uncrewed aerial systems for more consistent and objective measurements of airspace use by birds and bats. Optical systems, including visible-light cameras and thermal imagers, have expanded opportunities for automated monitoring [12-15]. However, the performance of these systems can be degraded by fog, precipitation, low light conditions, target occlusion, or system miscalibrations, and their effective range is generally limited to hundreds of meters [16]. Aerial surveys using optical imagers can provide broader-scale estimates of species distribution and abundance [17], but they represent only snapshots in time, may resample individuals along transects, are weather-dependent, can be costly, and generally provide limited information on flight trajectories.

Biologging technologies (e.g., animal-borne GPS and accelerometers) provide another approach for monitoring bird and bat movement by recording data directly from individuals. These devices can generate information on flight trajectories, habitat use, activity patterns, and in some cases, physiological or environmental conditions [18, 19], providing insight into behaviors that are difficult to observe directly, such as long-distance migration. Biologging can therefore complement remote sensing methods by linking movement patterns to known individuals, species, or life-history stages. However, biologger altitude estimates may be affected by sensor drift, atmospheric pressure variation, terrain correction, or geolocation uncertainty. Péron et al. [20] reported root mean square errors of between 4 and 42 m for a study comparing estimated altitude by four different biologgers to altitude at known geodesic points, and Lato et al. [21] presented mean errors of 25 m or more compared to laser altimetry. Further, biologging is constrained by battery life, tag recovery or data transmission requirements, and the logistical effort needed to capture animals. Consequently, biologging datasets are often limited to relatively small sample sizes that may not fully represent population level airspace use.

Ground-based radar (GBR) continuously tracks bird and bat movement over large spatial extents (order of kilometers), operating day and night under a wide range of environmental conditions [22]. GBR provides objective, automated measurements of a target's georeferenced location, speed, heading, and for 3D GBR systems, altitude, at high sampling rate. Advanced data analysis has further expanded the capabilities of GBR systems to provide estimates of relative target size, morphological characteristics, and even wingbeat frequency [23, 24]. These features make GBR well-suited for quantifying bird and bat movement patterns relevant to collision risk including spatial distribution, relative density, passage rate through zones occupied by infrastructure, migratory pathways [24, 25], behavioral responses such as attraction or avoidance, and temporal and spatial trends in these metrics.

Radar is a powerful tool, but it has important limitations [26]. Unlike human observers or imaging systems, radar alone cannot provide taxonomic identification of animals with certainty, and radar signals may be susceptible to interference ("clutter") from terrain, vegetation, sea surface modulations, insects, precipitation, or nearby infrastructure [27]. Advances in radar sensing, signal processing, and data analysis techniques (e.g., machine learning [28]), however, may facilitate taxonomic assessments and position GBR as critical technology for evaluating airspace use and collision risk for applications where continuous human observation and near-field optical monitoring are often logistically constrained, such as floating offshore wind energy projects.

GBR technology is increasingly being applied for pre-construction assessments, operational monitoring, migration and other ecological studies, and collision risk models [29, 30]. Despite its growing use, relatively few (if any) bird or bat studies have rigorously quantified GBR performance using controlled experiments with known target locations and trajectories. Nilsson et al. [31] cross-validated three different GBR systems but did not present validation with targets of known positions. Bunch & Herricks [32] presented a study that attempted to groundtruth an early avian GBR system. Qualitative assessments were made by comparing scope-facilitated, limited duration visual observations of birds at a preset distance and bearing from the radar unit. While the authors provided insights into factors affecting radar performance in tracking flying objects, quantitative metrics comparing visually observed target location and movement to radar measurements were not presented [32]. Without robust validation, uncertainty in GBR-derived observations can propagate into ecological analyses and risk assessments, limiting confidence in management decisions based on these data.

Here, we present validation of a commercially available 3D GBR system using controlled drone flights that simulated a range of biologically relevant flight behaviors. The specific objectives of this study were to: (1) calculate radar detection rate of drone flights across a range of conditions, (2) quantify differences between radar-derived target positions and known drone positions across three spatial dimensions, and (3) assess the conditions that affect the ability for radar to detect and track moving targets. The testing framework was designed to establish confidence in radar-derived target tracking data and to identify flight characteristics and operational considerations that may affect radar performance.

Materials and methods

Field Study

We validated the tracking performance of two DeTect, Inc. (Panama City, Florida, USA) 3D MERLIN® Bird and Bat Detection Radars (BDRs): (1) 7360 MERLIN BDR and (2) 9090 MERLIN BDR (hereafter, 7360 BDR and 9090 BDR) (Fig. 1). The 7360 BDR is a 360° radar with 45° beam (35° up and 10° down) and 2-3 km detection range, and the 9090 BDR is a 90° panel radar with 12.5° beam (6.25° up and down) and 6-8 km detection range. Both BDRs are solid-state, S-band, pulsed Doppler GBRs with 4 Hz update rate and minimum detectable velocity of 0.1 m/s. The radar unit is equipped with a multi-constellation Global Navigation Satellite System (GNSS) receiver and Attitude and Heading Reference System (AHRS) to facilitate georeferencing of radar-derived tracks.

Fig. 1. Materials and Methods. Left: MERLIN® Bird and Bat Radar Monitoring System. Right: Location of The Nature Conservancy's Jack and Laura Dangermond Preserve, Santa Barbara County, California, USA (yellow star) and map illustrating the deployment locations and viewsheds in which radar validation activities were conducted for the 7360 BDR in 2024 (gray square and arc) and 9090 BDR in 2026 (black dot and wedge).

GBR validation activities were primarily conducted at The Nature Conservancy's Jack and Laura Dangermond Preserve (the Preserve), Santa Barbara County, California, USA on 27 August 2024 and between 5 – 9 January 2026. The radar unit equipped with MERLIN® BDRs was deployed near Government Point in 2024 and at the “School House” in 2026 (Fig. 1). Only the 7360 BDR was activated and validated in 2024. It was centered at 0° (true north), covering flight heights from ground level to 175 m at a range of 250 m and up to 735 m altitude at a range of 1050 m. In 2026, validation activities were focused on the 9090 BDR. Its viewshed was centered at 200° from the School House, covering a swath from 155° to 245° (Fig. 1) and flight heights from ground level to 60 m altitude at a range of approximately 250 m from the radar to over 175 m altitude, 1250 m from the radar. The 9090 BDR viewshed in 2026 was partially obstructed by a dense tree line at a bearing of 170° from the radar system (**Fig. 1**), resulting in some eastern portions of drone flights being obscured and consequently, not tracked.

The 7360 BDR validation activities in August 2024 involved preprogrammed DJI Mavic 3 Enterprise drone flights in the shape of a cube (hereafter referred to as a “cube flight”) (Fig. 2A). Cube flights were designed to incorporate three primary movement patterns within a single flight, or cube:

- Transiting – predominantly horizontal movements with consistent altitude, simulating straight-line travel for evaluating radars’ ability to maintain continuous tracking over longer distances.
- Diving – characterized by vertical movement with minimal horizontal displacement, simulating steep descents (and ascents) and testing ability for radar to track targets with limited lateral motion.
- Turning – combined lateral and vertical movements as an intermediate between near-vertical diving movements and near-horizontal transiting movements.

These movement patterns allowed radar performance to be evaluated under a range of flight characteristics while maintaining a consistent programmed flight speed and repeatable flight pattern. Six cube flights were performed within the 7360 BDR viewshed, where cube dimensions were 100 m east to west (x), 100 m north to south (y; equivalent to range from radar), and 45 m to 50 m in altitude. The six cube flights were centered at 250, 400, 550, 700, 850, and 1000 m from the radar system. Wind speeds ranged between 5 m/s and 10 m/s on 27 August 2024 and conditions were foggy; relative humidity exceeded 80%.

Fig. 2. Radar Validation Flight Types. (A) Cube flight (transit to/from drone takeoff/landing location also shown), (B) transiting (rendering), (C) foraging, (D) dynamic soaring, and (E) chasing (rendering).

Two drones, DJI Mavic 2 and DJI Air 3, were used to simulate four classes of bird and bat flight behaviors in January 2026 (Fig. 2):

- Transiting – straight-line trajectories at consistent heading and altitude and sustained flight speed, reflecting purposeful travel between habitats.
- Foraging – complex, meandering trajectories with high path tortuosity, frequent directional changes at relatively low speeds, and repeated occupancy of localized airspace, consistent with area-restricted search behavior.
- Dynamic soaring – smooth, cyclic flight characterized by alternating ascents, descents, and banking turns with variable speed. This wind-assisted behavior is used by albatross, petrels, and some shearwaters [33-35].

- Chasing – high-speed, erratic flight with abrupt turns and repeated directional and speed adjustments, modeled after parasitic jaegers (*Stercorarius parasiticus*) [36] and was also aimed at mimicking bat foraging.

The Mavic 2 was used for manually controlled foraging and chasing flights, whereas the Air 3 was preprogrammed for transiting and dynamic soaring. These flights were conducted largely within the 9090 BDR viewshed at distances of 250 m to 1800 m from the radar unit (Fig. 1). Drone flight characteristics, e.g., altitude, speed, path length, bearing to radar, heading, and turn angles (where relevant) were varied across multiple flights of each flight class (17 transiting, 6 foraging, 55 dynamic soaring, and 2 chasing). Although the number of foraging and chasing flights performed was lower than other classes, the number of data points was comparable as these flights were each approximately 30 minutes in duration, compared to 3-5 minutes for the others. The sky was clear over the week of data collection and winds were primarily from the southeast. Wind speeds were less than 5 m/s on 6 and 9 January and ranged between 5 m/s and 25 m/s on 7 and 8 January 2026. Due to safety concerns, drones were not flown when sustained wind speeds exceeded 12 m/s.

To supplement field studies at the Preserve, a focused long-distance experiment was performed in Morro Bay, California, USA, on 19 June 2024. A DJI Mavic 2 was manually operated to mimic transiting (Fig. 2B) across distance range and flight height combinations of: 1.75–2.75 km at 60 m, 3–4 km at 60 m, 4–4.5 km at 40 m, 4–4.75 km at 60 m, and 4.5–5 km at 80–100 m. Due to physical obstructions, flights could not be extended beyond 5 km. These transiting flights were used to evaluate 9090 BDR detection rate at ranges greater than achievable at the Preserve.

Data Analysis

Hereafter, tracks recorded by the drones' onboard positioning systems (DJI Enterprise, Mavic, and Air use multi-constellation GNSS) are referred to as "drone tracks" and tracks recorded by radar are referred to as "radar tracks". The radar registers a separate track, consisting of a series of detections, for each object that moves through its field-of-view. Each detection within a single radar track is assigned a common identification number (hereafter referred to as a "Track ID") with detection time, latitude, longitude, altitude above sea level (ASL), distance from radar, and additional radar metrics. A single drone track is created for each drone flight and consists of timestamp, latitude, longitude, altitude (ASL), and other drone metrics at 10 Hz. Because the radar operates using Doppler principles, it requires continuous motion to maintain a track. If a target's radial velocity slows to less than 0.1 m/s or appears stationary during, e.g., an abrupt turn, the radar may lose tracking ability and then re-acquire it when motion appears to resume. Therefore, a single drone track could produce more than one radar track.

The following data preprocessing steps were necessary to match radar tracks to drone tracks for quantitative comparisons.

1. Target filtering. Radar tracks attributed to non-drone targets, such as birds, were identified and removed using: (A) RadView, project-developed software for isolating drone-associated radar tracks in 3D across user-defined time periods, spatial extents, and speed or (B) MERLIN® Display interface, which allows operators to positively identify and tag radar Track IDs of drone flights during operations. Filtered radar tracks were visually compared with corresponding drone tracks in ArcGIS Pro 3.6 (Esri; Redlands,

California) for data quality assurance (QA). Note that each detection associated with retained Track IDs were included in the analysis; isolated, spurious detections within a track were not removed.

2. Track joining. For cases where a drone flight produced multiple radar tracks, those individual tracks were merged into a single continuous radar track for comparison with the corresponding drone track. This resulted in six sets of matched drone-radar tracks of cube flights, along with 17 transiting, 6 foraging, 55 dynamic soaring, and 2 chasing sets of matched drone-radar tracks.
3. Coordinate transformation. Geographic coordinates recorded by drones and radars were transformed into a local Cartesian coordinate system (x, y) centered on the radar unit's location using a law-of-cosines spherical Earth approximation. Altitude was retained as a vertical coordinate (z; m ASL), and radar timestamps were converted from UTC to local time to align with drone data.
4. Track matching. Radar detections were recorded at irregular intervals of up to 0.2 s, whereas drone positions were at regular 0.1-s intervals, and small offsets between both timestamps could occur because the GBR system was synchronized to UTC using Network Time Protocol, while drone timestamps were recorded directly from GNSS signals. To enable direct comparison, both datasets were aligned to a common 0.1-s reference timeline. Drone positions were interpolated to this timeline, and radar positions were forward-filled to the nearest reference timestamp, allowing each radar detection to be paired with the nearest point on the corresponding drone trajectory.

Once each preprocessed and QA'ed radar track was assigned to each of the 86 drone tracks, radar performance metrics were quantified:

- Radar detection rate, defined as the proportion of the drone trajectory for which at least one radar detection occurred within a specified temporal window of the corresponding drone position. Temporal windows ranged from 1 s to 5 s to evaluate detection performance across time scales relevant to ecological and monitoring applications. Shorter temporal windows are most relevant for ecological questions requiring fine-scale information on behavioral responses. Longer windows may be appropriate when the primary question concerns broader-scale flight trajectories, relative activity, or occupancy of airspace. The ecological significance of each temporal window also depends on flight speed. For example, a songbird flying at 8 m/s would move 8 m during a 1-s window and 40 m during a 5-s window. For faster-flying birds, the same temporal windows correspond to proportionally longer travel distances, making temporal windowing an important consideration when relating radar performance to species, behavior, and the ecological or management question being addressed.
- Positional discrepancies. Root mean square deviation (RMSD) was calculated for the x, y, and z dimensions for matched drone-radar observations within each track:

$$RMSD_X = \sqrt{\frac{1}{n}\sum_{i=1}^{n}(X_{radar,i} - X_{drone,i})^2} \tag{1}$$

where $X_{radar,i}$ and $X_{drone,\,i}$ represent radar-estimated and drone-estimated position (x, y, or z) for the i-th matched observation within each track and n is the total number of matched observations per drone track. Track-level RMSD values were averaged across tracks, giving each drone track equal weight in summary statistics. In addition to RMSD, positional deviation (PD) and mean absolute positional deviation (MAD) were calculated for each paired drone-radar coordinate to evaluate biases and absolute differences, where:

$$PD_X = (X_{radar,i} - X_{drone,i}), \qquad (2)$$

$$MAD_X = \frac{\sum_{i=1}^{n} |X_{radar,i} - X_{drone,i}|}{n} \qquad (3)$$

Drone GNSS location uncertainties were estimated to be a maximum of 5 m in the horizontal plane (x, y) and 15 m in the vertical (z) [37].

Positional deviations were evaluated as a function of flight class, distance from radar (25-m bins), flight speed (1-m/s bins), and flight height (10-m bins), and detection rate was assessed as a function of flight class and temporal window. Data QA was conducted using ArcGIS and preprocessing and analyses were conducted in R [38].

Results

Detection rate

Cube flights recorded by the 7360 BDR exhibited the lowest median detection rate among the five flight behavior class categories, ranging from 42% to 59% for 1-s to 5-s temporal windowing (Fig. 3). Qualitative evaluation of detection rates across each of the six cube flights suggest that detection was slightly more reduced at the closest and furthest cubes, likely due to the drone transiting within the radar's "cone of silence" at close range (a conical blind spot directly above a GBR where the system cannot detect targets [39]) and decreased radar sensitivity at the farthest distances. Detection rates for chasing, foraging, dynamic soaring, and transiting (9090 BDR) exceeded 72% for 1-s temporal windowing, reaching median detection rates as high as 95% for dynamic soaring at 5-s temporal windowing (Fig. 3).

Fig. 3. Detection Rate by Flight Class and Temporal Windowing. Here, soaring = dynamic soaring.

The variability of detection rates was greater for dynamic soaring and transiting flights than for the other flight classes, which was due, in part, to the larger number tracks available for analysis. Several of these two flight classes exhibited detection rates below their respective medians (Fig. 3), indicating intermittent loss of track continuity rather than complete failure to detect the target. Chasing and foraging flights had narrower detection rate distributions, suggesting more consistent target detection across flights, although the number of tracks for these flight classes was smaller.

Detection rates presented in Fig. 4 were computed for flights performed at limited range relative to the 9090 BDR sensing capabilities. Therefore, detection rate of the 9090 BDR was estimated for five Mavic 2 transiting flights conducted at distances as far as 5 km from the radar in Morro Bay on 19 June 2024. With 1-s temporal windowing, the 9090 BDR detected the drone at rates of 85%, 64%, 63%, 70%, and 82% across distance range and flight height combinations of 1.75–2.75 km at 60 m, 3–4 km at 60 m, 4–4.5 km at 40 m, 4–4.75 km at 60 m, and 4.5–5 km at 80–100 m, respectively. Reduced detection between 3 and 4 km may have been due to difficulties in separating drone detections from those associated with high bird density (Fig. 4). Radar viewshed limitations likely affected the detection rate for 40 m flight height (i.e., 40 m was below the 9090 BDR beam); detection improved to 70% for the flight conducted at 60 m over a similar range and to 82% for flights at 80–100 m out to 5 km. These results indicate that the 9090

BDR can detect moving targets several kilometers from the radar, noting that detection performance at any range is affected by viewshed geometry.

Fig. 4. Signal Interference. High bird density recorded by the 9090 BDR during a transiting flight between 3 and 4 km from the radar. The DJI Mavic 2 drone flight path is denoted by yellow dots, radar detections are in magenta, and real birds are shown in blue. Inset: Location of long-distance radar performance testing in Morro Bay, California, USA (yellow star).

Positional discrepancies

Radar-derived positions were generally consistent with drone positions within tens of meters, although the magnitude and direction of positional discrepancies varied across spatial dimensions and among flight classes (Fig. 5, Fig. 6, and Fig. 7). Across different flight classes, the largest deviations were generally observed for cube flights (i.e., 7360 BDR observations), whereas foraging, dynamic soaring, and transiting flights recorded by the 9090 BDR exhibited comparatively smaller differences (Fig. 5). Chasing flights also exhibited relatively high horizontal discrepancies, with mean RMSD of approximately 16 m in the x-dimension and 14 m in both y and z (Fig. 6). Mean RMSD values for cube flights were approximately 23 m in the x- and z-dimensions and 13 m in y, compared with approximately 10–13 m in x and y and 10–15 m in the z-dimension for the foraging, dynamic soaring, and transiting flights recorded by the 9090 BDR (Fig. 6). Foraging and transiting flights had lower x-direction RMSD values (~10 m), while dynamic soaring exhibited the lowest RMSD value in the z-direction (~10 m).

Fig. 5. Root Mean Square Deviation (RMSD). RMSD (Eq. 1) between radar- and drone-derived positions for flight behavior classes along the (A) x-, (B) y-, and (C) z-dimensions (here, soaring = dynamic soaring).

Fig. 6. Mean RMSD. Mean of RMSD values shown in Fig. 5 across flight classes and spatial dimensions (here, soaring = dynamic soaring).

Fig. 7. Positional Deviation (PD) Distributions. PDs (Eq. 2) in the (A) x-, (B) y-. and (C) z-dimensions for flight behavior classes as indicated to the right of each row (soaring = dynamic soaring). Shaded regions denote estimated drone error of ±5 m in the horizontal and ±15 m in the vertical dimension.

The distribution of signed PDs indicated that discrepancies were not uniformly centered around zero and that the magnitude and direction of bias differed among flight classes (Fig. 7). In the x-dimension, cube flights exhibited a pronounced positive bias, whereas other behaviors showed predominantly negative deviations. The magnitude of x-direction bias was greatest for cube flights and chasing behavior, with median differences of approximately +12 m and −10 m, respectively, compared with median deviations of −5 m to −8 m for the other behaviors. In the y-dimension, the flight classes showed a slight positive bias. Cube flights again exhibited the largest median deviation (~+10 m), while median y differences for the remaining behaviors were approximately +5 m. In the z-dimension, cube flights exhibited the largest positive bias, with a median deviation of about +12 m, whereas the remaining behaviors were more closely centered around zero to +2 m.

PD distributions were generally concentrated near their respective median values, but extended tails of the distribution were present (Fig. 7). Individual PDs extended to approximately ±100 m, although these extreme values represented a small portion of the observations and are likely attributed to clutter (potentially real birds in the same air space as drones) or spurious detections in the case of cube flights. The broader PD distributions observed for cube flights (x- and z-dimensions) were consistent with their higher RMSD values and indicate greater variability in radar-derived positions relative to drone positions (Fig. 5).

MAD was found to vary as a function of distance from the radar, with patterns differing by flight class (and therefore, radar type) and spatial dimension (Fig. 8). Cube flights observed by the 7360 BDR showed the highest MAD values and were highly variable with distance from the radar, particularly in x- and z-directions. For the 9090 BDR observations, MAD values were generally lower and for the x- and y-dimensions, were more consistent with distance from radar. MAD for 9090 BDR data in the vertical plane increased from about 3 m at a range of 250 m from the radar to greater than 10 m at 1000 m from the radar (Fig. 8C). MAD for horizontal and vertical dimensions across the five flight behavior classes did not vary by more than a few meters across drone flight speeds of between 1 m/s and 15 m/s (data not shown).

Fig. 8. Mean Absolute Positional Deviation (MAD). MAD (Eq. 3) in the (A) x-, (B), y-, and (C) z-dimensions as a function of distance (25-m bins) from radar for each flight class. Dashed lines denote estimated drone error of 5 m in x- and y- and 15 m in the z-dimension and shading denotes 95% confidence interval.

Positional discrepancies were also evaluated as a function of drone flight altitude (meters ASL) and distance from radar for each flight class (Fig. 9). Results indicate that in general, deviations in the y-direction were generally within ±10 m and consistent with flight height and distance from radar (Fig. 9A). Deviations in the x- and z-directions, however, ranged from between −10 m to +35 m and −20 m to +40 m, respectively (Fig. 9B and Fig. 9C). Larger PD values were associated with cube and foraging flights, with largest deviations closest to the radar location for cube flights (i.e., near the cone of silence) and at lower flight altitudes and distances greater than 1000 m for foraging flights. The increase in z-dimension PD values with decreasing flight height and increasing distance from the radar for foraging and to a lesser extent, transiting (Fig. 9C), was likely associated with the limited vertical range of the 9090 BDR viewshed (12.5° beam) and decreasing terrain elevation from the radar location (50 m ASL) toward Government Point (<10 m ASL), which placed the drone near or just below the radar viewshed at greater distances for lower flight heights.

Fig. 9. Positional deviation (PD). PD (Eq. 2) in columns (A) x-, (B) y-, and (C) z-dimensions as a function of 10-m binned flight height and 25-m binned distance from radar averaged across tracks for each of the five flight classes, as labeled to the right of each row.

Discussion

Larger differences in the tracking performance of drones between cube flights (7360 BDR) and other flight classes recorded by the 9090 BDR are likely attributable to differences in radar signal power, which influences effective operating range, detection rate, track continuity, and overall positional accuracy. The 7360 BDR more frequently exhibited reduced track continuity during turns or rapid changes in target speed, with decreased detection rate and occasional generation of spurious detections at locations inconsistent with drone positions, at times with deviations of more than 200 m (Fig. 10). Although the 9090 BDR also occasionally lost targets during turns, spurious detections were not often observed immediately before target loss or after tracks were re-acquired.

Fig. 10. Radar Signal Loss and Spurious Detections. Example of radar signal loss and spurious detections during tight turns of a dynamic soaring flight. The drone track is shown in yellow and individual radar detections are shown as magenta dots.

Although median detection rates for transiting flights were comparable to those observed for other flight classes used to evaluate 9090 BDR performance, dynamic soaring and transiting flights exhibited the greatest variability in detection rate, with some flights falling below 50%. The lowest detection rates occurred when drone trajectories crossed perpendicular to the primary viewing direction of the 9090 BDR. Because Doppler radar sensitivity depends on the component of target motion directed toward or away from the radar, targets moving primarily across the radar beam have low to zero radial velocity and are therefore less likely to be tracked. In these cases, the radar temporarily lost the target as it crossed perpendicular to the beam centerline but re-acquired it shortly afterward. This viewing-geometry effect likely contributed to the reduced detection rates and greater track discontinuities observed for dynamic soaring and transiting flights that crossed normal to the center beam of the 9090 BDR.

Radar performance was also affected by flights characterized by rapid changes in direction and speed. The comparatively large positional discrepancies observed during chasing flights may reflect the combined effects of abrupt changes in heading and speed on radar track continuity. The tight turns, rapid accelerations, and directional changes of chasing trajectories likely resulted in temporary loss of targets and higher mismatches between the last pre-loss detection and first post-loss detection (see example in Fig. 10). This is consistent with higher RMSD and PD observed for chasing flights and suggests that pursuit-like, or foraging bat behaviors involving tight turns and rapid speed changes should be interpreted with greater caution than smoother trajectories.

In addition to radar tracking-related sources of discrepancy, systematic biases in radar positional deviations from drone positions may be attributable to uncertainty in the georeferenced position and orientation of the radar unit itself. Radar-derived target locations are calculated using the radar unit's GNSS-derived position and AHRS-derived attitude and heading, and radar signal measurements (slant range, horizontal azimuth angle, and vertical elevation angle). Offsets in the datum used for georeferencing radar tracks may therefore introduce systematic horizontal and/or vertical biases. For example, GNSS receiver altitude offsets could produce a direct shift in vertical datum and additional offsets that increase with range as the vertical error is projected over longer slant distances. Thus, even centimeter-scale uncertainty in radar unit lateral position, altitude, attitude, or heading can contribute to measurable differences in estimated flight altitude and/or horizontal positions that increase with range from the radar (e.g., Fig. 8C and Fig. 9C).

The magnitude of systematic bias observed for cube flights may also reflect differences in GNSS solution quality between deployments. Due to insufficient GNSS warm-up time (i.e., operator error) during the 7360 BDR cube flight validation in 2024, the radar's GNSS solution was based on fewer than 10 satellite fixes, whereas the 9090 BDR deployment in 2026 included more than 30 fixes. Lower satellite availability can degrade the precision of the radar reference position, thereby introducing errors in the radar unit location that are propagated into georeferenced target coordinates. This deployment-related difference provides a plausible explanation for the larger systematic positional biases observed in cube flights compared to the 9090 BDR results.

Although radar uncertainties can contribute to positional deviations between radar-derived tracks and drone locations, these discrepancies should also be interpreted in the context of uncertainty in the drone reference tracks. Drone positions, which were also derived from GNSS data, provide an independent but not error-free estimate of target location. Drone type (Enterprise 3, Mavic 2, or Air 3) was unlikely to have introduced systematic biases. The Mavic 2, applied for chasing and foraging flights, uses a combination of two satellite navigation systems (GPS and GLONASS); the Air 3 (dynamic soaring and transiting flights) uses three: GPS, Galileo, and BeiDou; and the Enterprise 3 (cube flights) GNSS receiver can access GPS, GLONASS, Galileo, and BeiDou. Despite the higher positional accuracy of the Enterprise 3, cube flights exhibited the highest discrepancies between drone and radar tracks, and the Mavic 2 and Air 3 produced consistent results across foraging and transiting flights, respectively. Nevertheless, positional discrepancies cannot be attributed solely to radar error but instead reflect the combined uncertainty of the radar- and drone-derived positions. Within this context, the observed vertical discrepancies for most 9090 BDR flight classes were generally comparable to the estimated drone vertical uncertainty (here, assumed to be ±15 m), indicating that radar-derived flight heights were sufficiently accurate for applications requiring classification of target altitude relative to ecologically or operationally important height bands.

These results are particularly relevant for wind energy risk assessments, where vertical accuracy is often the more consequential dimension for determining whether a target is flying below, within, or above a rotor-swept zone. The finding that vertical radar discrepancies were generally within or near the drone uncertainty threshold for 9090 BDR detections suggests that the radar can provide scientifically defensible information on flight height distributions for collision risk modeling. However, interpretation should remain conservative for flights involving abrupt turns, rapid speed changes or short track segments, or flights near the limit of a radar's viewshed; these conditions were found to result in more tracking discontinuities and positional variability as compared to other flight characteristics.

Summary and conclusions

This study presents a quantitative validation of a system of two 3D GBRs for tracking birds and bats. We performed controlled experiments with known drone positions and trajectories for a variety of biologically relevant flight classes. Both radars successfully detected moving targets and produced georeferenced tracks that were generally consistent with drone positions within tens of meters. Radar-derived target positions in the vertical dimension were mostly within drone positional errors (±15 m). Radar detection performance was strongest for the 9090 BDR and was reduced for flights near the limits of the radar viewshed. Positional discrepancies were influenced by both radar tracking continuity, largely affected by behaviors involving abrupt turns or rapid changes in speed, and georeferencing uncertainty, including potential imprecision in radar unit position, attitude, and heading.

These findings highlight the need for careful siting and accurate georeferencing of data from observational assets such as GBR. Tracks near the edge of the radar viewshed, trajectories perpendicular to the radar beam, or flights characterized by dynamic maneuvering should be interpreted with caution. With these considerations addressed, GBR provides quantitative assessments of bird and bat presence/absence, relative abundance, and 3D movement patterns at spatial and temporal scales that are unattainable using other tools. It is important to note that radar performance is not static; ongoing advances in system design and signal processing are expected to reduce limitations described in this study. For example, since this study was completed, the DeTect, Inc. 7360 BDR has been upgraded with higher signal power and should enhance detection sensitivity and track continuity.

Accurate, validated radar observations provide a robust foundation for assessing wildlife interactions with a broad range of anthropogenic infrastructure, enabling more defensible collision risk assessments, improved environmental monitoring, and science-based decision making wherever birds and bats interact with the built environment. As infrastructure development continues to expand globally, validated remote sensing technologies such as GBR for ecological studies will play an increasingly important role in balancing infrastructure needs with wildlife conservation.

Acknowledgements

This project was supported by the California Energy Commission Electric Program Investment Charge (Award No. EPC-23-001). The authors acknowledge the Jack and Laura Dangermond Preserve (https://doi.org/10.25497/D7159W), Point Conception Institute, The Nature Conservancy, and California State Parks for their support of this research. Special thanks to Javier Vidao, Dana Delew, Carolyn Belak, Sharon Hsu, Gene Revelas, Marcus Chevitarese, Scott Terrill, and Michael Burns, who provided valuable insights and assistance with fieldwork. This effort benefited greatly from input by Garry George and Chris Haney (National Audubon Society), Cris Hein (National Laboratory of the Rockies), Yi-Hui Wang, David Pereksta, and Scott Johnston.

Conflict of Interest

Jesse Lewis currently serves as the President of DeTect, Inc., provider of the ground-based radar technologies evaluated in this study. As an employee and executive officer, Mr. Lewis holds financial interests in DeTect, Inc. To mitigate potential bias, the drone flights, data processing, statistical analyses, and interpretation of results were independently conducted and verified by all other authors, who declare that they have no known competing financial interests or personal relationships that could have appeared to influence the work reported in this paper.

Author Contribution

GC conceived the original idea, designed the methodology, and wrote the original draft of the manuscript. JPS performed formal analysis, validated data, and curated data and software. SS helped conceptualize the research, performed formal analysis, developed methodologies, and wrote sections of the original draft of the manuscript. RY and LC made contributions to data curation and formal analysis. SK helped conceive of the study idea and contributed to development of the methodology. JL and FS performed field investigations and developed methodologies. All authors contributed to the review and editing of the manuscript.

Data Availability

Datasets and code used during this study are publicly available on GitHub: Pettis Schallert, J. (2026). 3d-radar-validation-birds-bats [Code and Dataset]. GitHub. https://github.com/IntegralEnvision/3d-radar-validation-birds-bats

References

1. Manville AM. Impacts to birds and bats due to collisions and electrocutions from some tall structures in the United States: wires, towers, turbines, and solar arrays – State of the art in addressing the problem. In: Angelici F, editor. Problematic Wildlife. Switzerland: Springer International Publishing; 2016. pp. 415-442. https://doi.org/10.1007/978-3-319-22246-2_20
2. Zwart MC, McKenzie AJ, Minderman J, Whittingham MJ. Conflicts between birds and on-shore wind farms. In Angelici F, editor. Problematic Wildlife. Switzerland: Springer International Publishing; 2016. pp. 489-504. https://doi.org/10.1007/978-3-319-22246-2_23
3. Loss SR, Lao S, Eckles JW, Anderson AW, Blair RB, Turner RJ. Factors influencing bird-building collisions in the downtown area of a major North American city. PLOS One. 2019; 14: e0224164. https://doi.org/10.1371/journal.pone.0224164

4. Elmore JA, Hager SB, Cosentino BJ, O'Connell TJ, Riding CS, Anderson ML et al. Correlates of bird collisions with buildings across three North American countries. Conserv. Biol. 2021; 35: 654-665. https://doi.org/10.1111/cobi.13569
5. Van Doren BM, Willard DE, Hennen M, Horton KG, Stuber EF, Sheldon D, et al. Drivers of fatal collisions in an urban center. Proc. Natl. Acad. Sci. 2021; 118: e2101666118. https://doi.org/10.1073/pnas.2101666118
6. Santander F, Morant J, Perez-Garcia JM. Bird and bat mortality at wind farms in South America: Lessons learned from monitoring and mitigation practices in Chile. J. Environ. Manag. 2026; 398: 128420. https://doi.org/10.1016/j.jenvman.2025.128420
7. Baasch DM, Hegg AM, Dwyer JF, Caven AJ, Taddicken WE, Worley CA, et al. Mitigating avian collisions with power lines through illumination with ultraviolet light. Avian Conserv. Ecol. 2022; 17: 9. https://doi.org/10.5751/ACE-02217-170209
8. O'Malley KD, Schofield HW, Wright PGR, Hargreaves D, Corcoran AJ, Mathews F. Increasing canopy cover elevates vehicle collision risk for barbastelle bats (*Barbastella barbastellus*) at roads. Sci. Rep. 2025; 15: 37011. https://doi.org/10.1038/s41598-025-14315-2
9. Brighton CH, Portugal SJ, Taylor GK. Bio-informed blade patterns for mitigating bird collisions with wind turbines. J. R. Soc. Interface, 2026; 23: 20250719. https://doi.org/10.1098/rsif.2025.0719
10. Lawson RR, O'Connell TJ, Elmore JA, Riding CS, Riggs GJ, Loss SR. Window markers reduce bird-window collisions in a real-world application. Ornithol. Appl. 2026; duag047. https://doi.org/10.1093/ornithapp/duag047

11. Koger B, Hurme E, Costelloe BR, O'Mara MT, Wikelski M, Kays R, et al. An automated approach for counting groups of flying animals applied to one of the world's largest bat colonies. Ecosphere. 2023; 14: e4590. https://doi.org/10.1002/ecs2.4590

12. Matzner S, Warfel T, Hull R ThermalTracker-3D: A thermal stereo vision system for quantifying bird and bat activity at offshore wind energy sites. Ecol. Inform. 2020; 57: 101069. https://doi.org/10.1016/j.ecoinf.2020.101069

13. Robinson Willmott J, Forcey GM, Vukovich M. New insights into the influence of turbines on the behavior of migrant birds: implications for predicting impacts of offshore wind developments on wildlife. J. Phys. Conf. Ser. 2023; 2507: 012006. https://doi.org/10.1088/1742-6596/2507/1/012006

14. Amichai E, Forcey GM, Vukovich M, Robinson Willmott J. Multi-sensor arrays provide complementary information on bat presence and activity in the offshore environment. J. N. Am. Bat Res. 2025; 1: 75-88.

15. Cook A. Review of Aberdeen Bay collision monitoring data. Report for Project No. SPO03. The Biodiversity Consultancy. 2026; 29 pp.

16. Chang G, Kramer S, Lewis J, Chevitarese M, Cheung L, Haluza R, et al. SEABIRD: System for Environmental Assessment of Bird/Bat Interactions with Real-Time Detection. California Energy Commission, Energy Research and Development Division. 2026; Publication Number: CEC-500-2026-[###].

17. Hatch SK, Connelly EE, Divoll TJ, Stenhouse IJ, Williams KA. Offshore observations of eastern red bats (Lasiurus borealis) in the mid-Atlantic United States using multiple survey methods. PLOS One. 2013; 8: e83803. https://doi.org/10.1371/journal.pone.0083803

18. Ripperger SP, Carter GG, Page RA, Duda N, Koelpin, A, Weigel R. Thinking small: Next-generation sensor networks close the size gap in vertebrate biologging. PLOS Biol. 2020; 18: e3000655. https://doi.org/10.1371/journal.pbio.3000655

19. Ellis-Soto D, Flack A, Strandburg-Peshkin A, Wild TA, Williams HJ, O'Mara MT. From biologging to conservation: Tracking individual performance in changing environments. Proc. Natl. Acad. Sci. U.S.A. 2025; 122: e2410947122. https://doi.org/10.1073/pnas.2410947122

20. Péron G, Calabrese J M, Duriez O, Fleming CH, García-Jiménez R, Johnston A, et al. The challenges of estimating the distribution of flight heights from telemetry or altimetry data. Anim. Biotelem. 2020; 8. https://doi.org/10.1186/s40317-020-00194-z

21. Lato KA, Stepanuk JEF, Heywood EI, Conners MG, Thorne LH. Assessing the accuracy of altitude estimates in avian biologging devices. PLOS One. 2022; 17: e0276098. https://doi.org/10.1371/journal.pone.0276098

22. Stepanian PM, Chilson PB, Kelly JF. An introduction to radar image processing in ecology. Methods Ecol. Evol. 2014; 5: 730-738. https://doi.org/10.1111/2041-210X.12214

23. Mirkovic D, Stepanian PM, Kelly JF, Chilson PB. Electromagnetic model reliably predicts radar scattering characteristics of airborne organisms. Sci. Rep. 2015; 6: 34537. https://doi.org/10.1038/srep35637

24. Werber Y, Sextin H, Yovel Y, Sapir N. BATScan: A radar classification tool reveals large-scale bat migration patterns. Methods Ecol. Evol. 2023; 0: 1-16. https://doi.org/10.1111/2041-210X.14125

25. Mein S, Nebel S. The use of radar in the study of animal migration. Nat. Educ. Knowl. 2012; 3: 76.

26. Hüppop O, Ciach M, Diehl R, Reynolds DR, Stepanian PM, Menz MHM. Perspectives and challenges for the use of radar in biological conservation. Ecography. 2018; 42: 912-930. https://doi.org/10.1111/ecog.04063

27. Jones AL, McCann DL, Mitchell LJ, McIlvenny J, Williamson BJ. Autonomous radar ornithology: Benchmarking automated bird detection and tracking. IET Radar, Sonar Navig. 2025; 20: e70163. https://doi.org/10.1049/rsn2.70163

28. Stratton C, Chang G, Archer E, Young R, Spada F, Kramer SH, et al. Machine learning classification of Pacific seabird flight behavior using three-dimensional ground-based Doppler radar. Ecol. Inform. 2026; submitted.

29. Dempsey L, Clerc J, Hein C. New frontiers in wind-wildlife monitoring systems. Biol. Conserv. 2025; 311: 111449. https://doi.org/10.1016/j.biocon.2025.111449

30. Shultz A, Solick D, Whitby M, Newman C, Corcoran A. Integrating 3-D thermal videography, ultrasonic acoustics, and weather radar to characterize bird and bat activity at wind turbines. PLOS One. 2025; 21: e0352329. https://doi.org/10.1371/journal.pone.0352329

31. Nilsson C, Dokter AM, Schmid B, Scacco M, Verlinden L, Backman J, et al. Field validation of radar systems for monitoring bird migration. J. Appl. Ecol. 2018; 55: 2552-2564. https://doi.org/10.1111/1365-2664.13174

32. Bunch W, Herricks EE. Observational validation of avian radar systems. Atlantic City, NJ, USA: Proceedings of the 2010 FAA Worldwide Airport Technology Transfer Conference. 2010; 12 pp.

33. Paiva VH, Guilford T, Meade J, Geraldes P, Ramos JA, Garthe S. Flight dynamics of Cory's shearwater foraging in a coastal environment. Zoology. 2009; 113: 47-56. https://doi.org/10.1016/j.zool.2009.05.003

34. Ainley DG, Porzig E, Zajanc D, Spear LB. Seabird flight behavior and height in response to altered wind strength and direction. Mar. Ornithol. 2015; 43: 25-36.

35. Kempton JA, Wynn J, Bond S, Evry J, Fayet HA, Gillies N, et al. Optimization of dynamic soaring in a flap-gliding seabird affects its large-scale distribution at sea. Sci. Adv. 2022; 8. https://doi.org/10.1126/sciadv.abo0200

36. Bélisle M, Giroux JF. Predation and kleptoparasitism by migrating parasitic jaegers. The Condor: Ornithol. Appl. 2015; 97: 771-781. https://doi.org/10.2307/1369185

37. Garrido-Carretero MS, Azorit C, de Lacy-Perez de los Cobos MC, Manuel Valderrama-Zafra J, Carrasco R, Gill-Cruz AJ. Improving the precision and accuracy of wildlife monitoring with multi-constellation, multi-frequency GNSS collars, J. Wildl. Manag. 2023; 87: e22378. https://doi.org/10.1002/jwmg.22378

38. R Core Team. R: A Language and Environment for Statistical Computing (Version 4.2.1). R Foundation for Statistical Computing. 2022. Available from: https://www.R-project.org/

39. Kollias P, Bharadwaj N, Widener K, Jo I, Johnson I. Scanning ARM cloud radars: Part 1: Operational sampling strategies. J. Atmos. Ocean. Tech. 2014; 31: 569-582. https://doi.org/10.1175/JTECH-D-13-00044.1

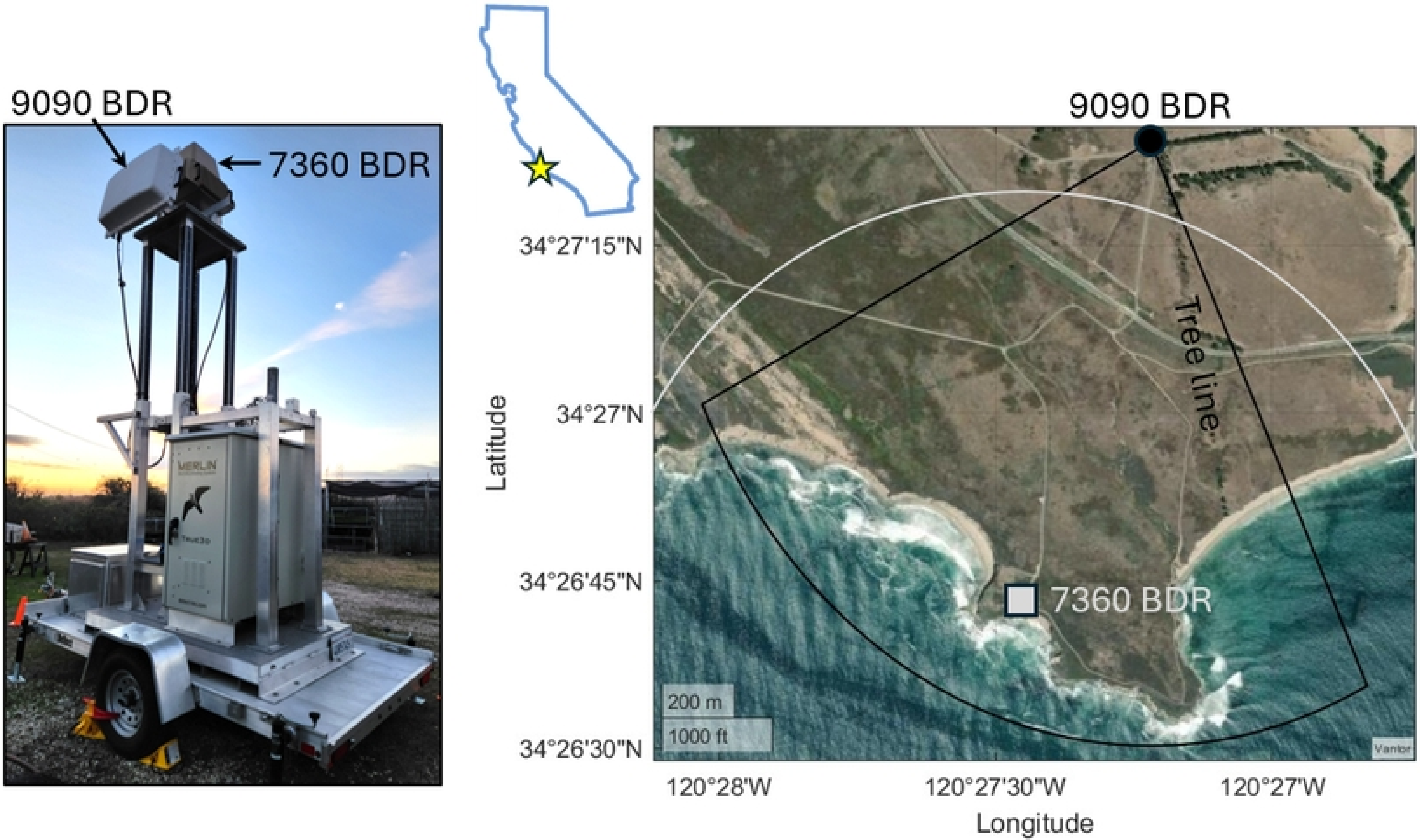

9090 BDR
7360 BDR
MERLIN
9090 BDR
Tree line
7360 BDR
200 m
1000 ft
Vantor
34°27'15"N
34°27'N
34°26'45"N
34°26'30"N
Latitude
120°28'W
120°27'30"W
120°27'W
Longitude

Figure 1

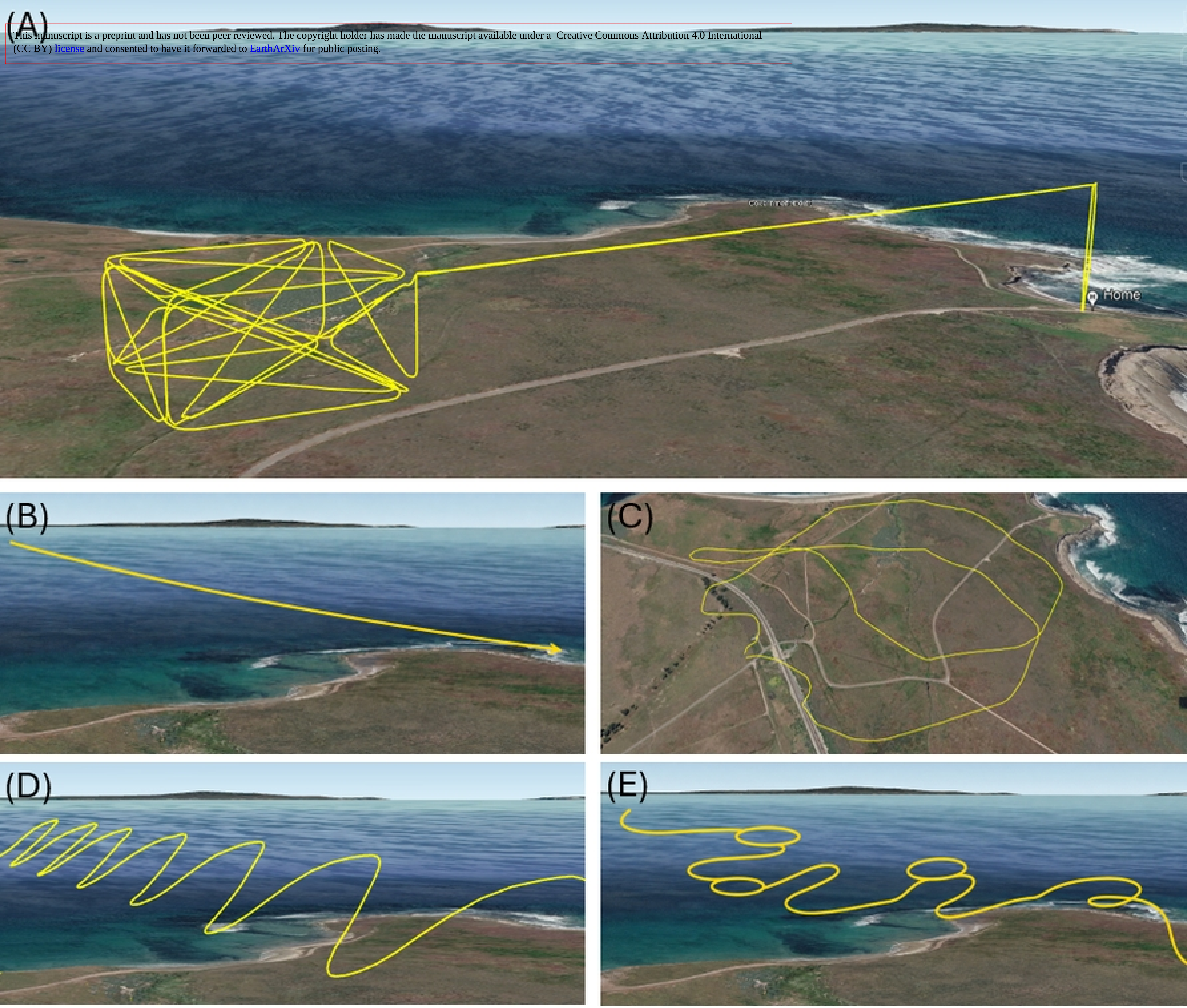

Figure 2

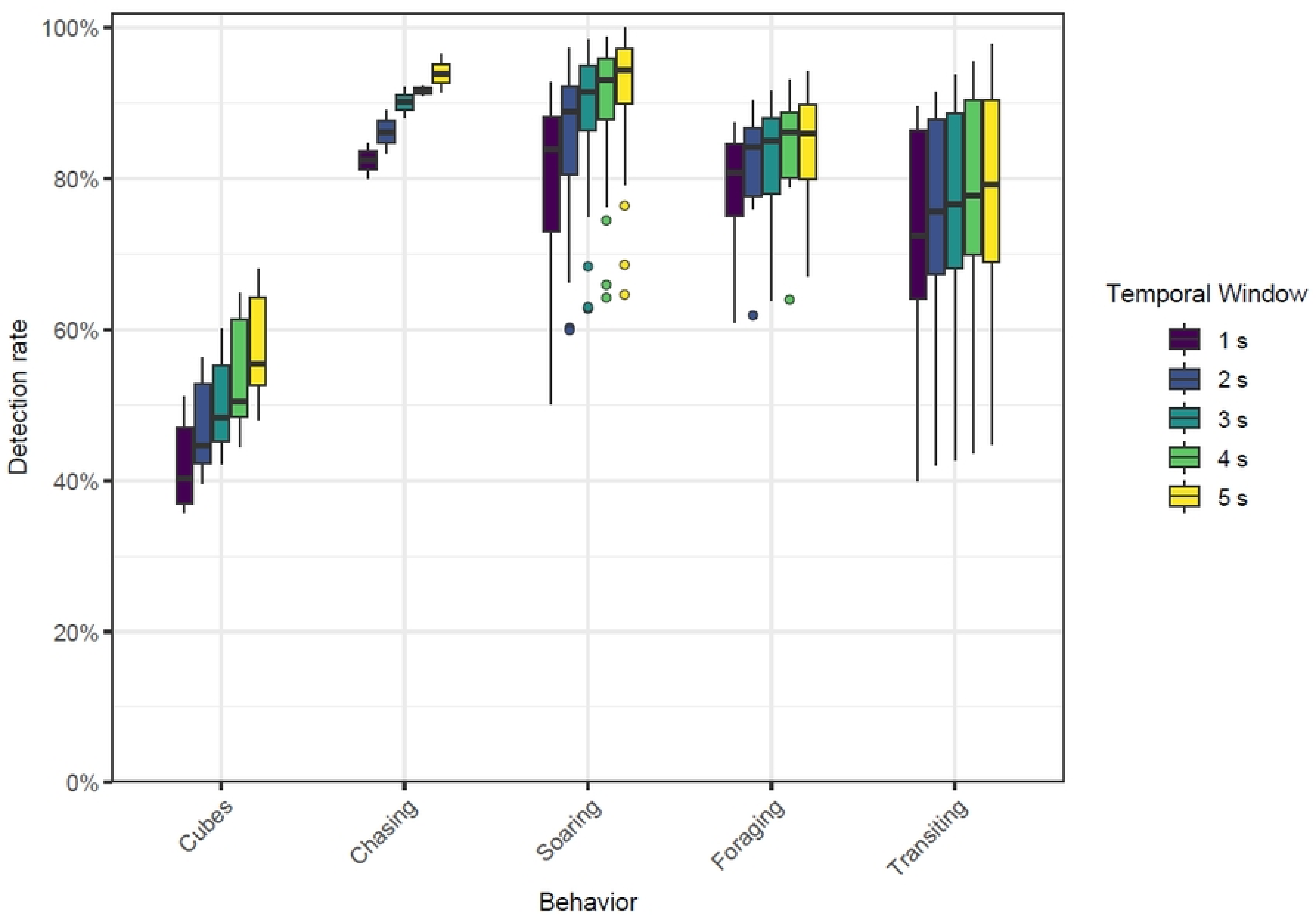

100%
80%
60%
40%
20%
0%
Detection rate
Cubes
Chasing
Soaring
Foraging
Transiting
Behavior
Temporal Window
1 s
2 s
3 s
4 s
5 s

Figure 3

Figure 4

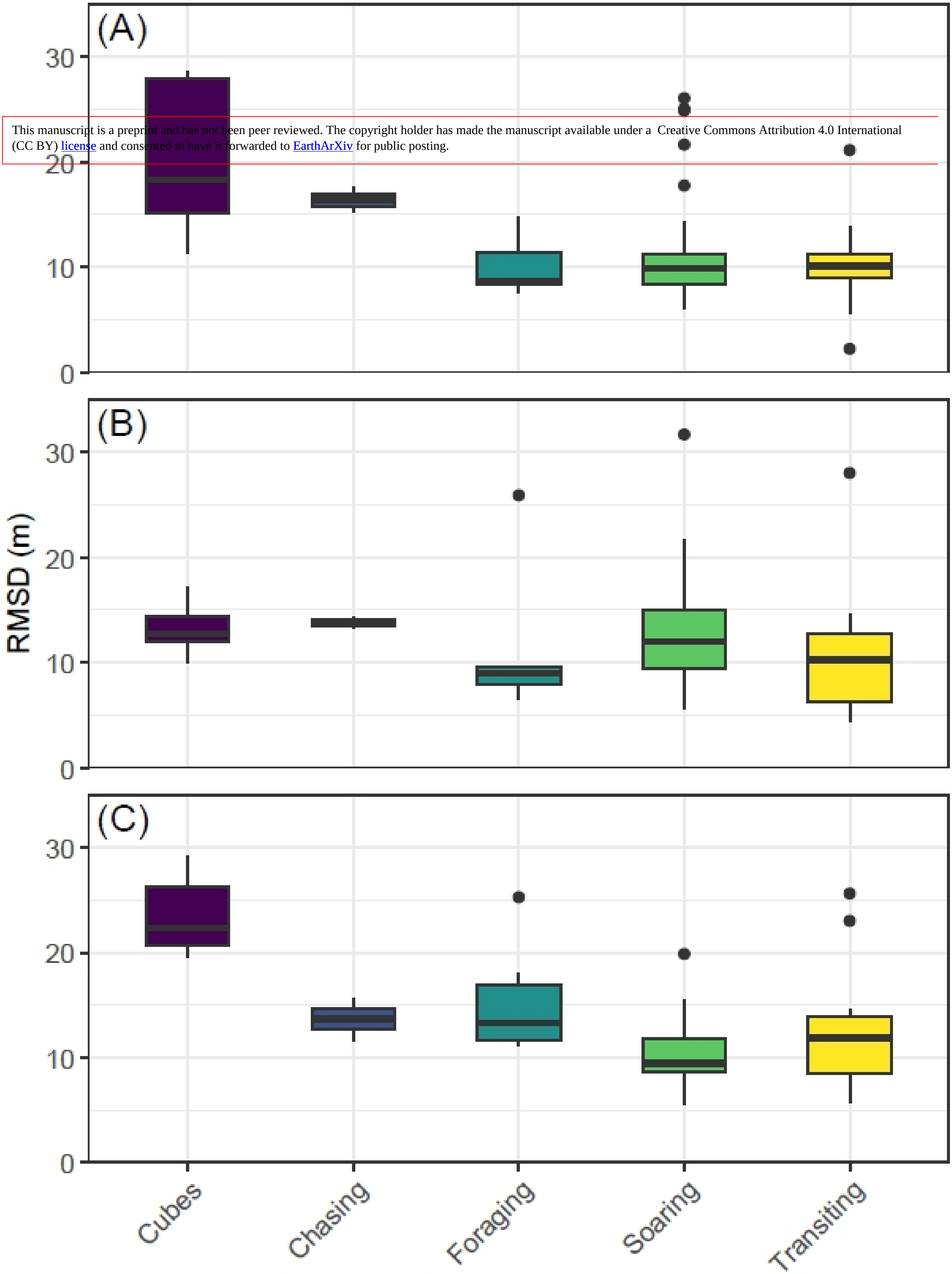
(A)
(B)
(C)
RMSD (m)
0
10
20
30
Cubes
Chasing
Foraging
Soaring
Transiting

Figure 5

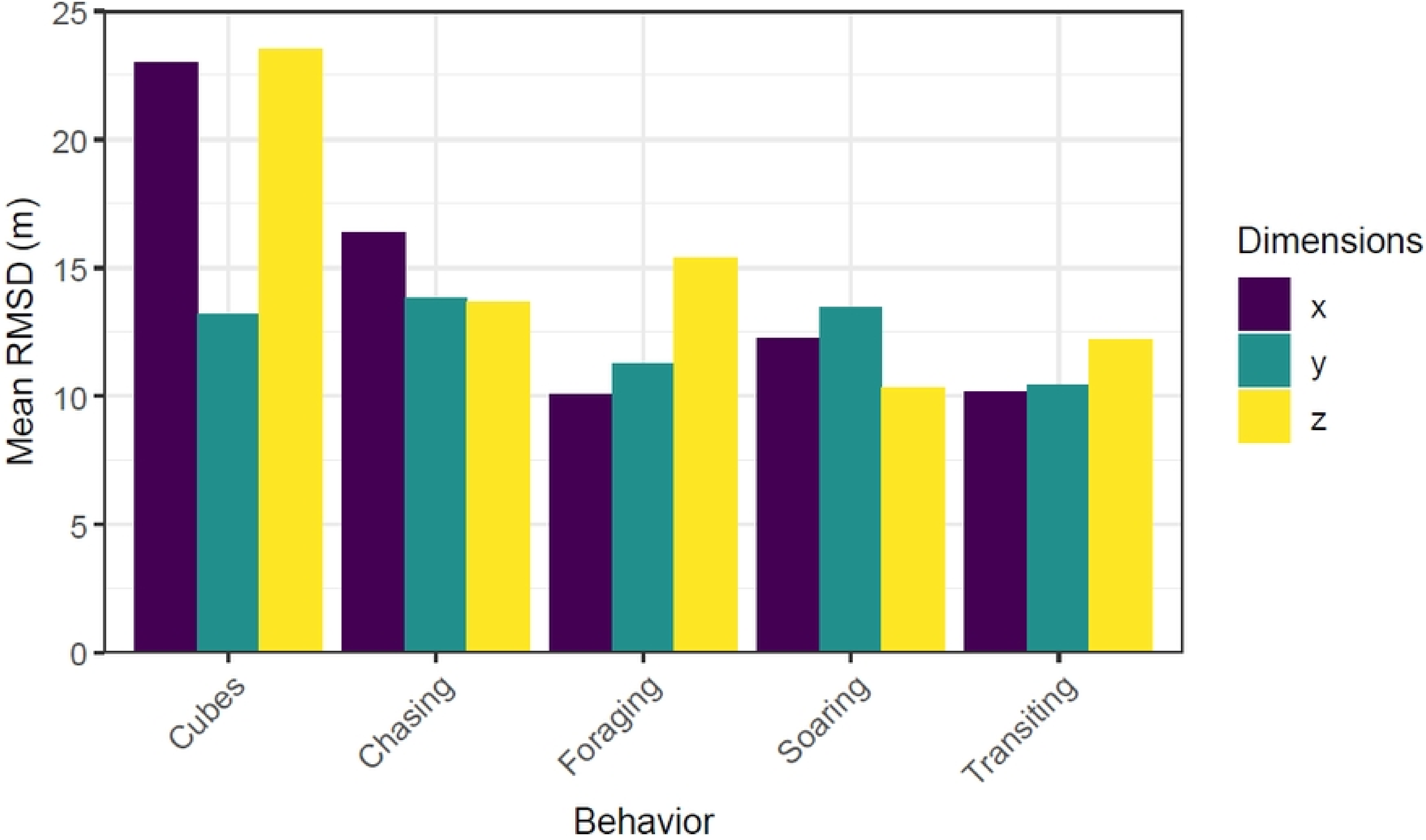

Mean RMSD (m)
25
20
15
10
5
0
Cubes
Chasing
Foraging
Soaring
Transiting
Behavior
Dimensions
x
y
z

Figure 6

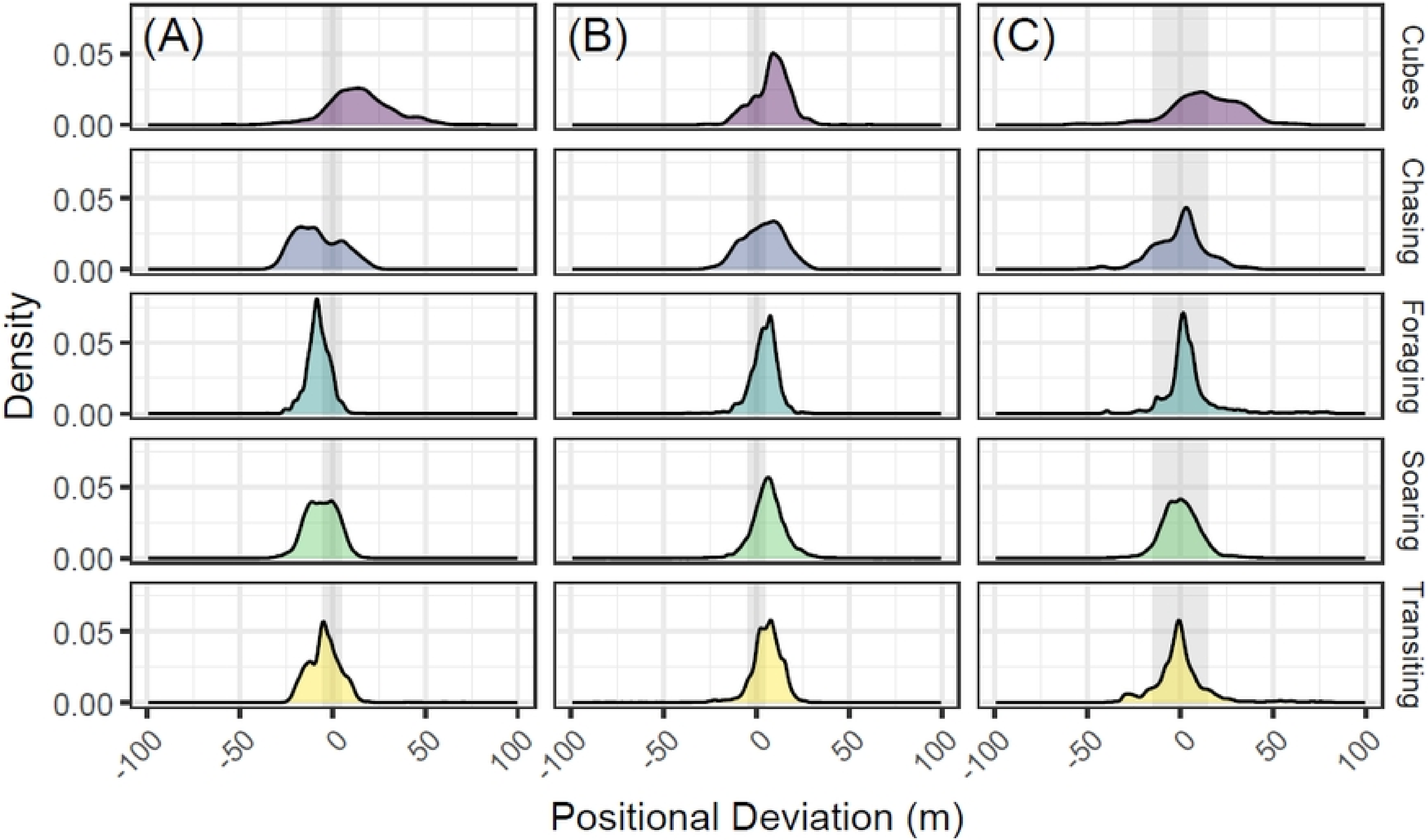
(A)
(B)
(C)
Cubes
Chasing
Foraging
Soaring
Transiting
Density
0.05
0.00
-100
-50
0
50
100
Positional Deviation (m)

Figure 7

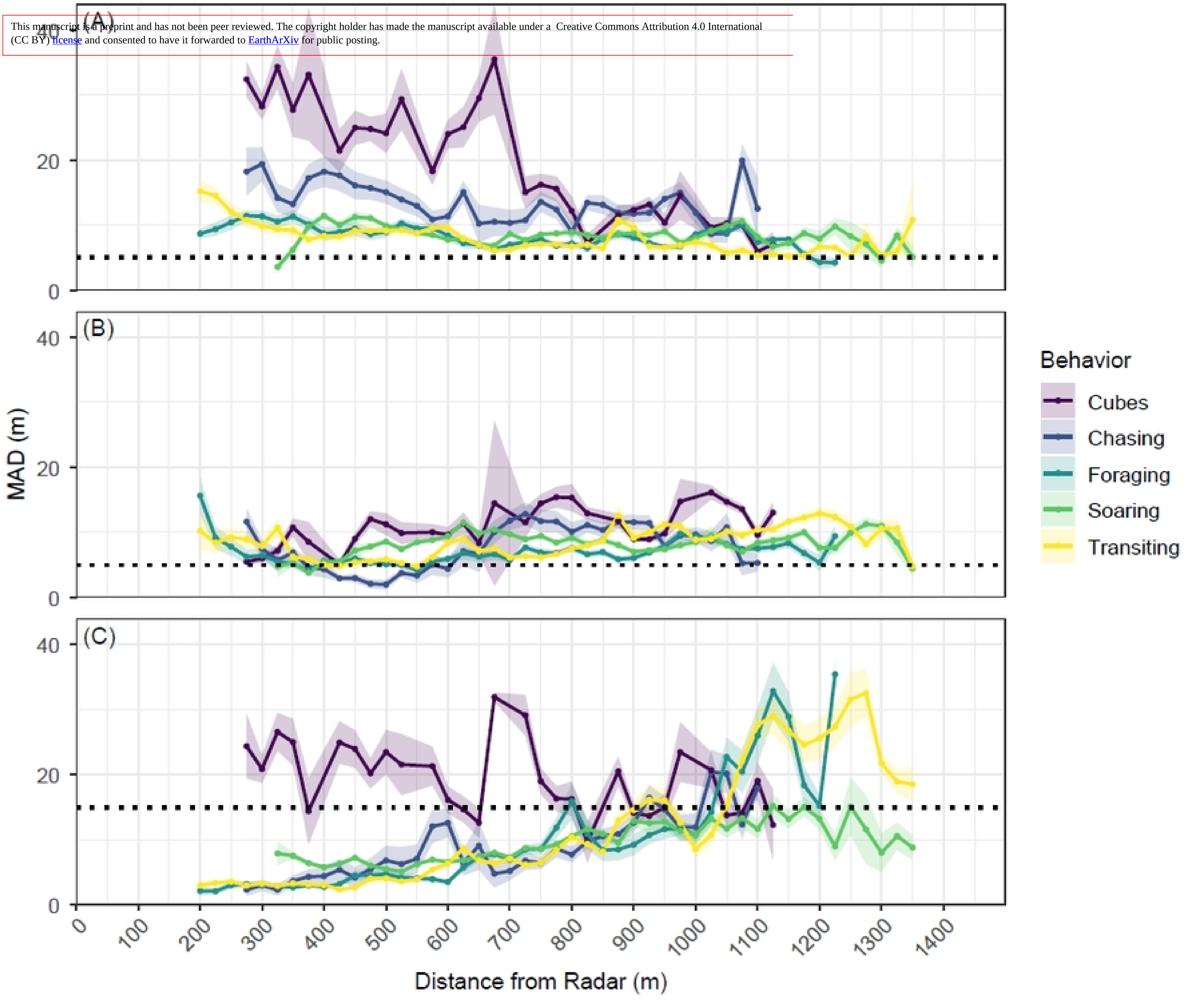

(A)
(B)
(C)
0
20
40
MAD (m)
0
100
200
300
400
500
600
700
800
900
1000
1100
1200
1300
1400
Distance from Radar (m)
Behavior
Cubes
Chasing
Foraging
Soaring
Transiting

Figure 8

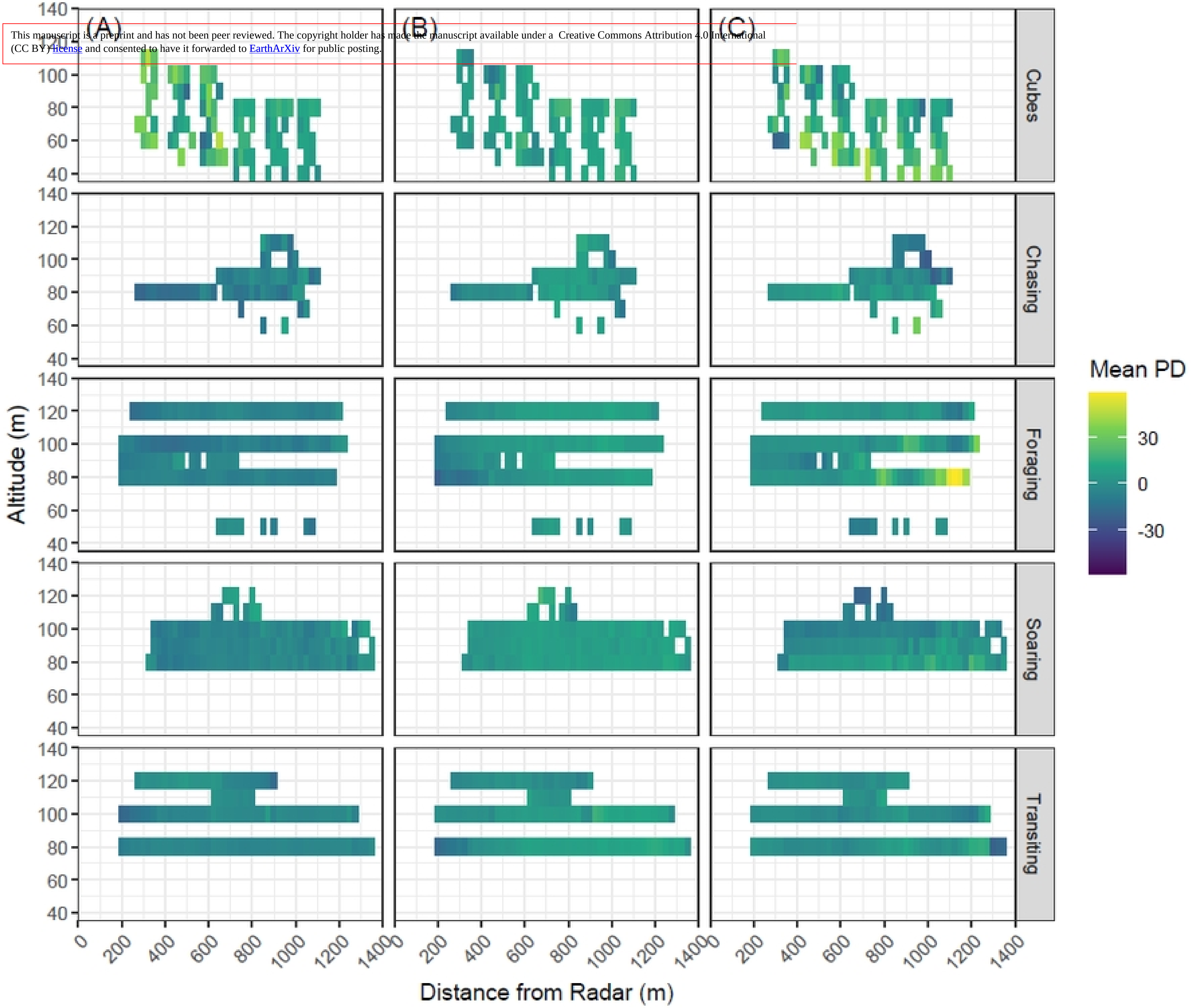
(A)
(B)
(C)
Cubes
Chasing
Foraging
Soaring
Transiting
Altitude (m)
Distance from Radar (m)
Mean PD
30
0
-30
140
120
100
80
60
40
0
200
400
600
800
1000
1200
1400

Figure 9

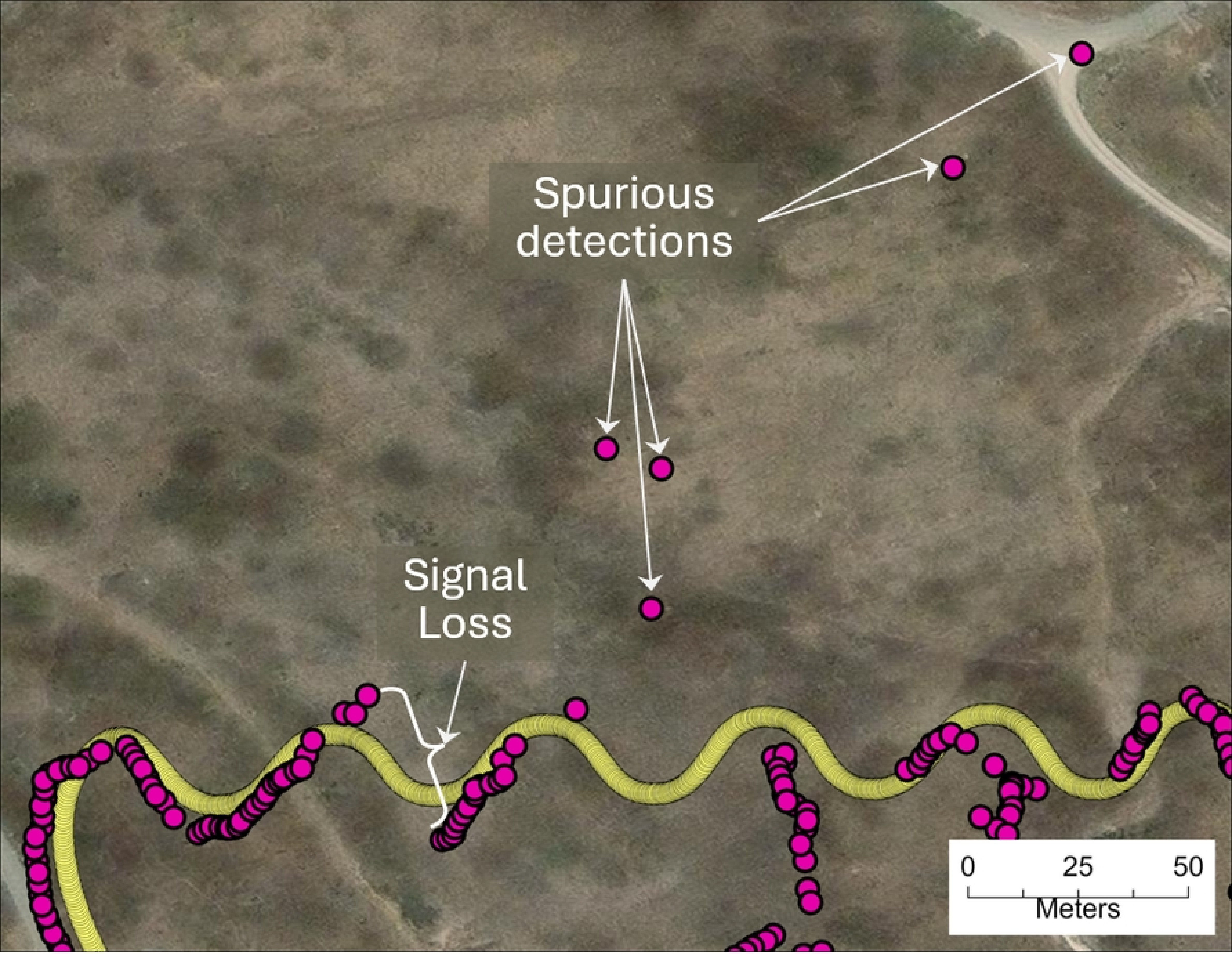

Figure 10